SAND--~~95E 5711C~~
Conf-940945--8 95-8502C

Modeling the Segregation of Hydrogen to Lattice Defects in Nickel

James E. Angelo, N.R. Moody, and M.I. Baskes, Sandia National Laboratories, Division 8712, Livermore, CA 94550

Abstract:

In order to better understand the effect of hydrogen on the fracture behavior of nickel, this study uses the embedded atom method (EAM) to model the segregation of hydrogen to lattice defects in nickel. The dislocations modeled include an edge, a screw, and a Lomer dislocation in the locked configuration, i.e. the Lomer-Cottrell Lock (LCL). Several coincident site lattice boundaries are also investigated, these being the $\Sigma 3(112)$ and $\Sigma 11(113)$ tilt boundaries. It will be shown that the trap site energies in the vicinity of both the edge and screw dislocations is only about 0.1 eV while for the LCL and all of the grain boundaries the maximum trap site energy in the vicinity of the defect is on order 0.3 eV. Using a Monte-Carlo method to a impose a hydrogen environment produces much stronger segregation of hydrogen to the deeper traps. When compared to recent experimental studies showing that a binding energy between 0.3-0.4 eV is required for trap site controlled fracture in IN903, it can be concluded that the embrittlement process is most probably associated with trapping of hydrogen to the Lomer-Cottrell Locks.

Introduction:

Hydrogen is known to have a detrimental effect on grain boundary fracture characteristics of metals such as iron as well as iron and nickel based superalloys [1-4]. However fundamental aspects of the embrittlement process have not been fully defined due to the complex nature of the material interactions. In particular, the question arises: *How does hydrogen affect the fracture process?*. There are many theories of how the embrittlement process may occur, see both [5] and [6] for reviews of the possible mechanisms. Of these, two have received considerable attention. The first model proposes that hydrogen promotes a decrease in the cohesive strength of the material. This model is termed the hydrogen enhanced decohesion model (HEDE). The second model suggests that the failure occurs do to an increase in the local plasticity near a crack tip. This model is termed the hydrogen enhanced localized plasticity model (HELP). Both models have support in the experimental community, [1-5,7,8] for HEDE and [6,9-11] for HELP, as well as the theoretical community [12-15] for HEDE and [16-18] for HELP. Since both processes can occur concurrently, relating the failure process to one or the other mechanism may be a difficult task at best. By using the EAM it is possible to predict the trap site binding energy of hydrogen to various defects in nickel. It is also possible to model the room temperature segregation behavior of hydrogen to these defects. This may shed light on the possible mechanisms for hydrogen enhanced failure.

In this paper, the embedded atom method (EAM) is used to model the effect of room temperature segregation of hydrogen to various defects in a nickel lattice. The EAM is used to determine the energetics of the Ni-H system with Monte-Carlo simulations applied to study the trapping of hydrogen to the various lattice defects in nickel. In section I, the EAM and Monte-Carlo (MC) methods used in this study are described. Section II describes the defects, both dislocations and tilt boundaries, that are produced in the nickel lattice and segregation behavior of hydrogen to each type of defect. Section III presents a discussion of how the results of this study can help in understanding the effects of hydrogen on material behavior is presented.

DISCLAIMER

Portions of this document may be illegible in electronic image products. Images are produced from the best available original document.

I. The Embedded Atom Method

The embedded atom method (EAM) [19-21] is an empirical scheme which allows for modeling large numbers of atoms in metallic systems. It has met with great success in modeling both bulk and defect properties in these systems, see [21] for many applications of this method. A new parameterization of the interaction of hydrogen and nickel is used in this study [22]. The parameters were fit to a wide range of properties for the Ni-H system. In particular, the stacking fault energy of nickel is reasonably well represented by this parameterization. This allows for producing the various dislocation structures investigated in this study. In previous studies [12-14], the predicted stacking fault energy of nickel was low so that it was difficult to study the interaction of hydrogen with dislocations. It is important that the interaction of hydrogen with dislocations be addressed since in almost all of the models for hydrogen enhanced failure, the interaction of hydrogen with the dislocations plays a crucial role.

The EAM can be combined with Monte-Carlo simulations [23,12-14] to determine the equilibrium distribution of atoms in metallic systems. This is accomplished by performing a number of steps, called Monte-Carlo steps, each of which can create or destroy atoms (in this study only hydrogen can be created or destroyed) or cause the random motion of an atom. In this study, a given Monte-Carlo step is always accepted when the change in energy is favorable, i.e. the step results in a decrease in total energy. If the energy is increased by a given Monte-Carlo step, the step is accepted with a probability given by Boltzmann statistics for the given temperature. By averaging over several million to several tens of millions of Monte-Carlo steps reasonable statistics can be developed so that distributions of atoms in thermal equilibrium with the environment can be produced.

II. Results

In this study, several dislocation and grain boundary structures in nickel were investigated. The dislocations investigated were an edge dislocation with line direction, $\mathbf{l} = [\bar{1}12]$, and Burgers vector $\mathbf{b} = a/2[110]$, a screw dislocation with $\mathbf{l} = [110]$, $\mathbf{b} = a/2[110]$, and finally a Lomer dislocation with $\mathbf{l} = [1\bar{1}0]$, $\mathbf{b} = a/2[110]$. In all cases, the initial displacement field of the dislocations was generated using anisotropic elasticity theory [24]. These atomic positions were then used as the starting configuration for the EAM calculations. For all of the dislocation geometries the simulation cell for the atomistic calculations was a cylinder with the axis along the dislocation line. Periodic boundary conditions were applied along the dislocation line with the periodic repeat distance being approximately 1.0 nm depending upon the dislocation geometry. The cylinder had a radius of 5.0 nm with the dislocation core being near the center of the cylinder. For the edge dislocation the simulation cell consisted of 6205 atoms while for both the screw and Lomer dislocations the simulation cell consisted of 7204 atoms. In order to keep the dislocation from leaving the simulation cell, the outer shell of radius 1.0 nm was held fixed during the energy minimization. As might be expected, both the edge and screw dislocations showed a planar dissociation on the <111> glide plane. The separation of the partials was approximately 2.5 nm for the edge dislocation and 1.0 nm for the screw dislocation. These separations are consistent with the fault energy of 90 ergs/cm^2 predicted by the potential used in this study. The boundary conditions had little effect on the results as starting the atomistic simulations from a configuration where the partials were dissociated had little or no effect on the calculated energies or positions of the atoms.

The relaxed edge dislocation structure is shown in figure 1(a). The core positions are indicated by the light balls. For the screw dislocation, the relaxed dislocation configuration is shown in figure 2(a), with the core atoms again indicated. By placing a single hydrogen atom in an octahedral site in the vicinity of these dislocations, the trap site energy could be determined. Here, the trap site energy is defined as the difference in energy for the relaxed system with a hydrogen atom in an octahedral site near the dislocation and the energy of the relaxed perfect lattice with a hydrogen atom in a

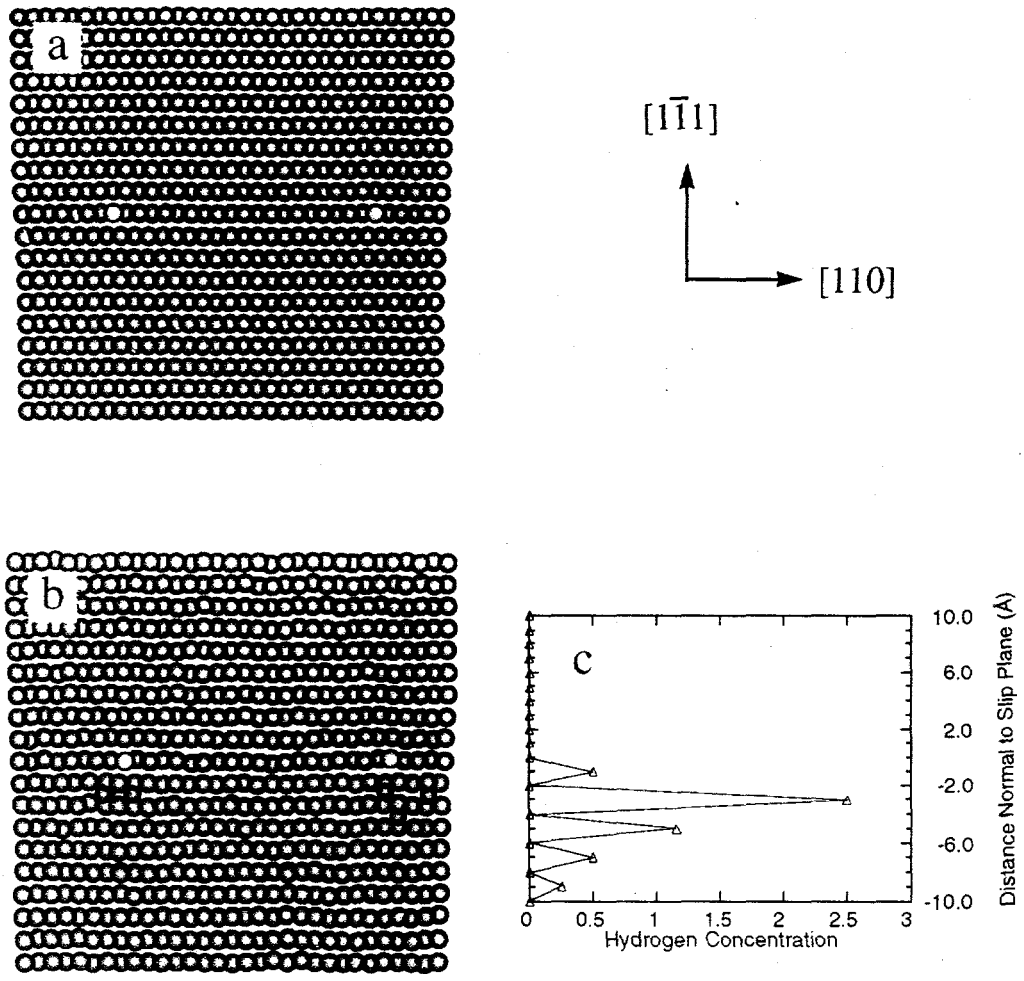

Figure 1: (a) The relaxed atomic structure of an edge dislocation in nickel showing the dislocation has separated into partials separated by a stacking fault. (b) The effect of room temperature segregation of hydrogen to the edge dislocation for a far-field hydrogen concentration of 446 appm. The core of the dislocations are indicated by the light balls. Hydrogen is indicated by the small balls. (c) The equilibrium hydrogen concentration profile averaged over 10 million MC steps.

octahedral site. It was found that the maximum trap energy for a hydrogen near the dislocation was approximately 0.12 eV for the edge dislocation and 0.09 eV for the screw dislocation which is in excellent agreement with the experimentally measured binding energy (0.09 eV) of hydrogen to dislocations in nickel [25]. In both cases the strongest

trap was not at the core but displaced by about 0.2-0.3 nm from the core position. The relaxed dislocations were then exposed to a hydrogen environment using the Monte Carlo method described above. Far-field hydrogen concentrations of both 23±15 and 446±30 appm at 300 K were simulated for this study. The approximate far-field hydrogen concentrations were calculated by averaging the number of hydrogen atoms in the simulation cell over approximately 50-80 million Monte-Carlo steps. The large error bars on the far-field hydrogen concentration of 23 appm is due to the relatively poor statistics.

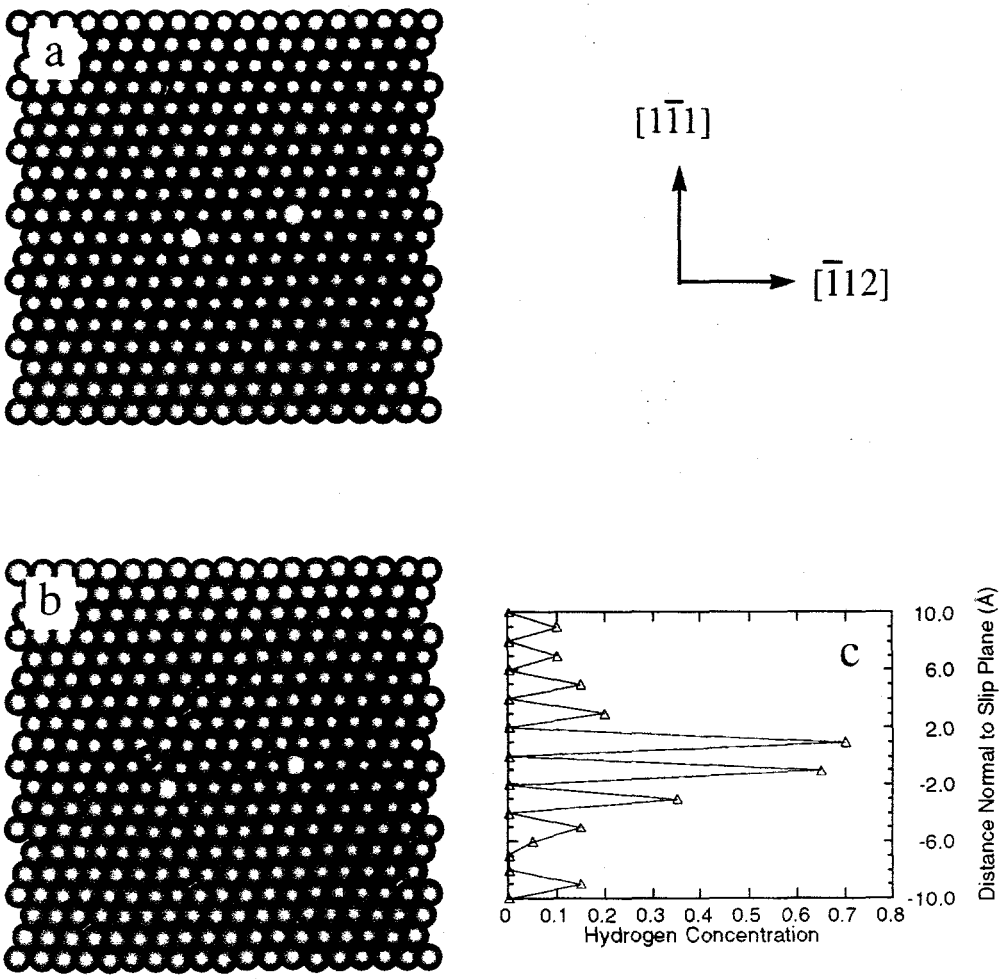

Figure 2: (a) A screw dislocation in nickel dissociated by approximately 1.0 nm. This produces a tensile strain field near each partial dislocation. (b) The segregation behavior of hydrogen to the dissociated screw dislocation for a far-field hydrogen concentration of 446 appm showing a single hydrogen atom. A hydrogen atom is observed in the tensile strain field of one of the partials. (c) Concentration profile for the image shown in (b) averaged over 10 million MC steps. The core of the dislocations are indicated by the light balls and hydrogen is indicated by the small ball.

The segregation of hydrogen to the edge dislocation for a far-field hydrogen concentration of 446 appm is shown in figure 1(b). The hydrogen is indicated by the small balls in this figure. This figure shows the atomic structure near the dislocation for one particular configuration of the Monte-Carlo simulation. The concentration of hydrogen near the dislocation is increased above that for the perfect lattice. To compare

the concentrations trapped at the dislocation to those in the far-field, the number of hydrogen atoms in the simulation cell averaged over approximately 10 million Monte-Carlo steps was compared to the number of hydrogen atoms expected in the same volume of a perfect lattice. This gives the solubility enhancement (C/C_0) near the dislocation. For all of the dislocations the volume used was defined by a cylinder of radius of 3.5 nm surrounding the dislocation. For all the distance along the cylinder was determined by the periodic length of the simulation cell (approximately 1.0 nm for all of the dislocations). For the far-field hydrogen concentration of 446 appm, the solubility enhancement is 5.2. The solubility enhancement does not accurately describe where the hydrogen is in relation to the dislocation since in fact all of the hydrogen is trapped in the tensile strain field of the dislocation. The segregation behavior is clearly indicated in figure 1(c) which plots the concentration of hydrogen as a function of distance normal to the slip plane. These profiles were again averages over 10 million MC steps. The peaks in the hydrogen concentration which occur approximately every 0.2 nm is simply a reflection of the (111) inter-planar spacing. This figure clearly shows all of the segregated hydrogen is present in the tensile region below the fault plane. This is because the extra half plane for each partial dislocation creates a state of compressive stress in the upper half of the figure. It is also observed that the hydrogen does not segregate strongly to the stacking fault; it only has a trap binding energy of 0.075 eV to the fault for the given potential set [22]. At the far-field hydrogen concentration of 23 appm little hydrogen was trapped at the edge dislocation.

For the screw dislocation, the trapped hydrogen at far-field hydrogen concentration of 446 appm is shown in figure 2(b). A single hydrogen is observed trapped in the tensile strain field of one of the partial dislocations. This reflects the fact that hydrogen is trapped to opposite sides of the partial dislocations. The concentration profile shown in figure 2(c) gives an indication of this phenomena. It shows an increase in the hydrogen concentration at the stacking fault as well as above and below the fault plane by one (111) plane spacing. The hydrogen trapped above the fault plane was almost always immediately above the partial dislocation shown on the left of Fig 2(b). Similarly almost all of the hydrogen trapped below the fault plane was trapped below the partial dislocation on the right of figure 2(b). This trapping behavior can be rationalized by noting that the perfect screw dislocation does not produce a hydrostatic stress. When the dislocation dissociates to partial dislocations with Burgers vectors of the type a/6<112>, each partial dislocation has an edge component of Burgers vector. The edge component is opposite for the two partial dislocations so that the compressive and tensile stress fields for each occur on opposite sides of the slip plane. For the given far-field hydrogen concentration (446 appm), the solubility enhancement was 2.32 over that in the far-field. Comparison of this solubility enhancement to the solubility enhancement for the edge dislocation indicates that the screw dislocation, even after dissociation, is a significantly weaker trap for hydrogen than the edge dislocation. For the far-field hydrogen concentration of 23 appm no hydrogen was trapped at the screw dislocation.

The Lomer dislocation was generated in a perfect configuration with $\mathbf{l} = [1\bar{1}0]$, $\mathbf{b} = [110]$, and a slip plane of (001). Thus for this dislocation to move by glide, it must either dissociate in the (001) plane or not dissociate at all. After relaxation, the simulations showed that the dislocation dissociated by the reaction $\mathbf{b} = a/2[110] > \mathbf{b} = a/6[112] + SF + \mathbf{b} = a/6[110] + SF + \mathbf{b} = a/6[11\bar{2}]$. In this case the a/6<112> Shockley partials have moved by glide on nonparallel {111} glide planes. The dislocation arrangement shown in figure 3 has been predicted as a strain hardening mechanism in fcc metals and is called a Lomer-Cotrell Lock (LCL) [26]. It is termed a locked dislocation since the dissociation is non-planar and the dislocation can not move by glide on it's primary (001) glide plane. This dislocation arrangement is important since it is likely to occur in material systems where dislocation slip bands intersect. When dislocations

moving on nonparallel <111> glide planes intersect they could form this locked configuration. This intersection would then act as a stress concentrator as subsequent dislocations gliding on the same slip planes pile-up against the LCL. The relaxed Lomer dislocation, in the locked configuration, is shown in figure 3(a). The core atom positions are shown as the light atoms. This figure shows the nonplanar configuration of this dislocation. In this figure, it can be seen that the core of the a/6[110] dislocation exhibits a large volume defect. Thus the Lomer dislocation might be a more

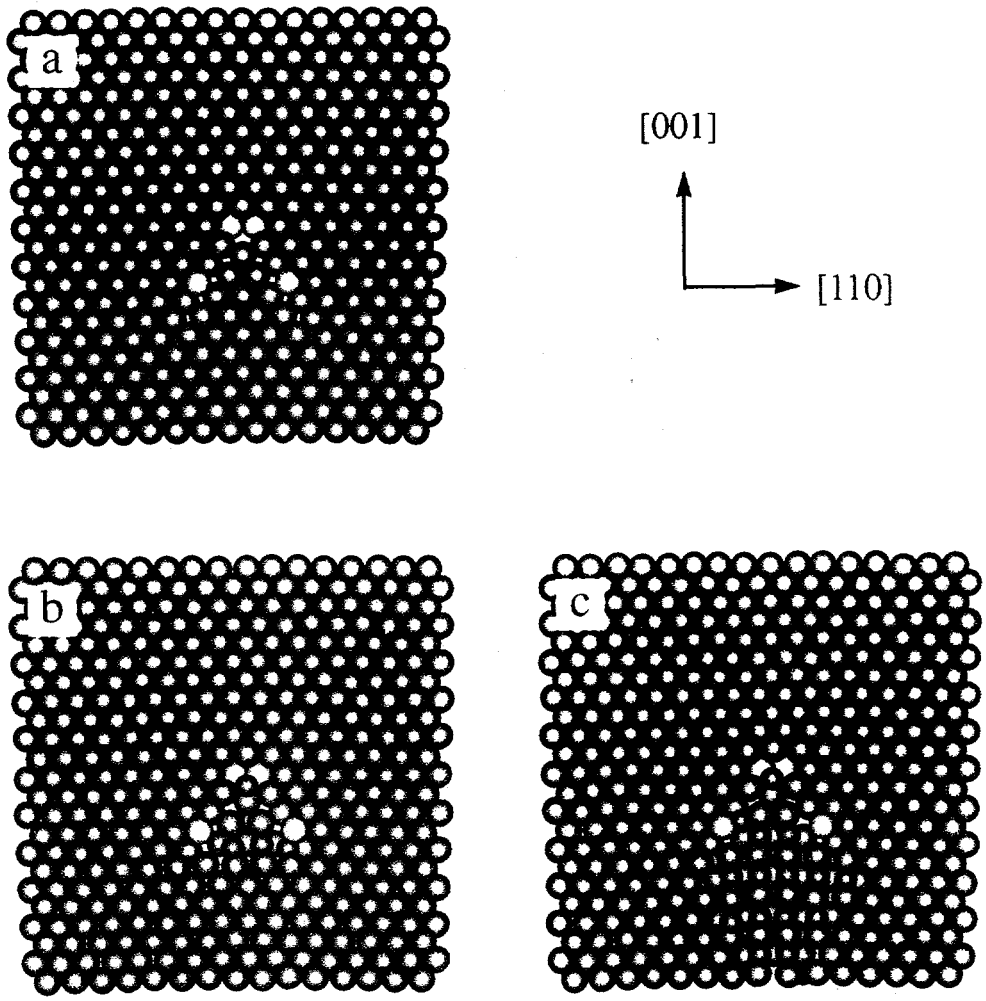

Figure 3: The structure of a dissociated Lomer dislocation is shown in (a). This configuration is termed a Lomer-Cottrell Lock (LCL) since the dislocation cannot move by glide on the (001) slip plane. (b) and (c) show the effect of exposing this dislocation to a far-field hydrogen concentration of 23 and 446 appm, respectively. The core of the dislocations are indicated by the light balls and hydrogen is indicated by the small balls.

effective trap for hydrogen than is the edge dislocation, which has the same edge component of Burgers vector but does not exhibit such a large volume defect at the dislocation core (see Fig. 1(a)). In fact, the maximum trap site energy for hydrogen to the

LCL is at the core of the a/6[110] dislocation with a binding energy of 0.33 eV which is approximately 3 times larger than for the edge or screw dislocations. At a far-field hydrogen concentration of 23 appm, the LCL traps a significant amount of hydrogen as is shown in figure 3(b). The concentration of hydrogen is increased by a factor of 300 over that in the far-field. The results of exposing the Lomer dislocation to a far-field hydrogen concentration of 446 appm is shown in figure 3(c). There is a further increase in the amount of hydrogen trapped at this dislocation. Here the amount of hydrogen trapped at the dislocation is 75 times greater than in the far-field. These figures both show that hydrogen is not trapped in the region below the dislocation - outside the slip planes of the Shockley partials. This dissociated configuration has caused the compressively strained region to extend below the overall glide plane.

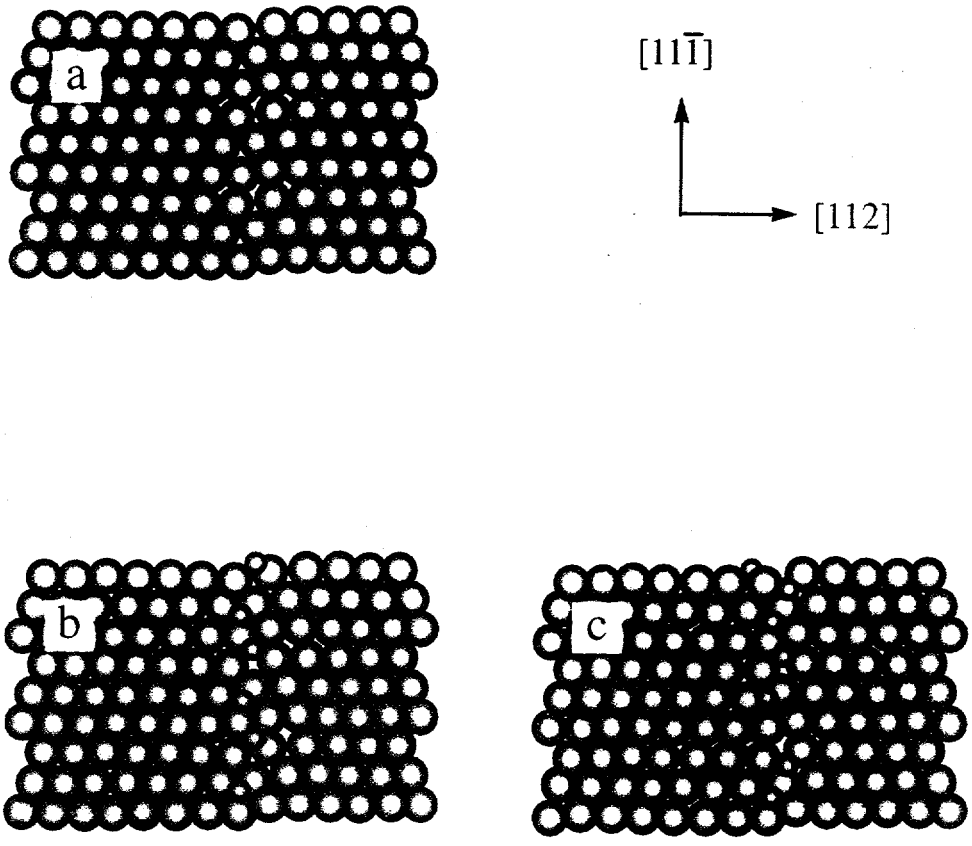

Figure 4: (a) The minimum energy structure of a Σ3(112) tilt boundary in nickel is asymmetric. (b) and (c) show the effect of exposing the tilt boundary structure to far-field hydrogen concentrations of 23 appm and 446 appm, respectively. High energy trap sites at the boundary fill at the low far-field concentration. The asymmetry in the boundary structure is clearly mimicked in the asymmetric segregation behavior exhibited in figure (c). In (b) and (c) hydrogen is indicated by the small balls.

Next the trapping of hydrogen to various tilt boundaries in nickel was investigated. The boundaries explored in this study were the Σ3(112) and Σ11(113) tilt boundaries. The Σn(jkl) notation [27] indicates that every 1/n atoms is coincident between the two lattices with the boundary plane being (jkl). The Σ3 tilt boundary was

formed by rotating two grains about a common <110> tilt axis with the boundary plane parallel to {112}. Similarly, the $\Sigma 11$ boundary was formed by rotating the grains around a common <110> direction and joining the crystals along a {113} plane. Both of the boundaries generated in this study consisted of a cell containing approximately 1000 atoms. Periodic boundary conditions were applied along the tilt axis and normal to the boundary plane. Parallel to the boundary plane the lattices extend by 3.0 nm on both sides. Since the relaxed boundary structures determined in this study were obtained by energy minimization at 0K, the relaxed structure may not be the minimum energy configuration. This is because if the system is near a local minimum which is separated from the global energy minimum by a sufficient energy barrier, the system will not relax to the global

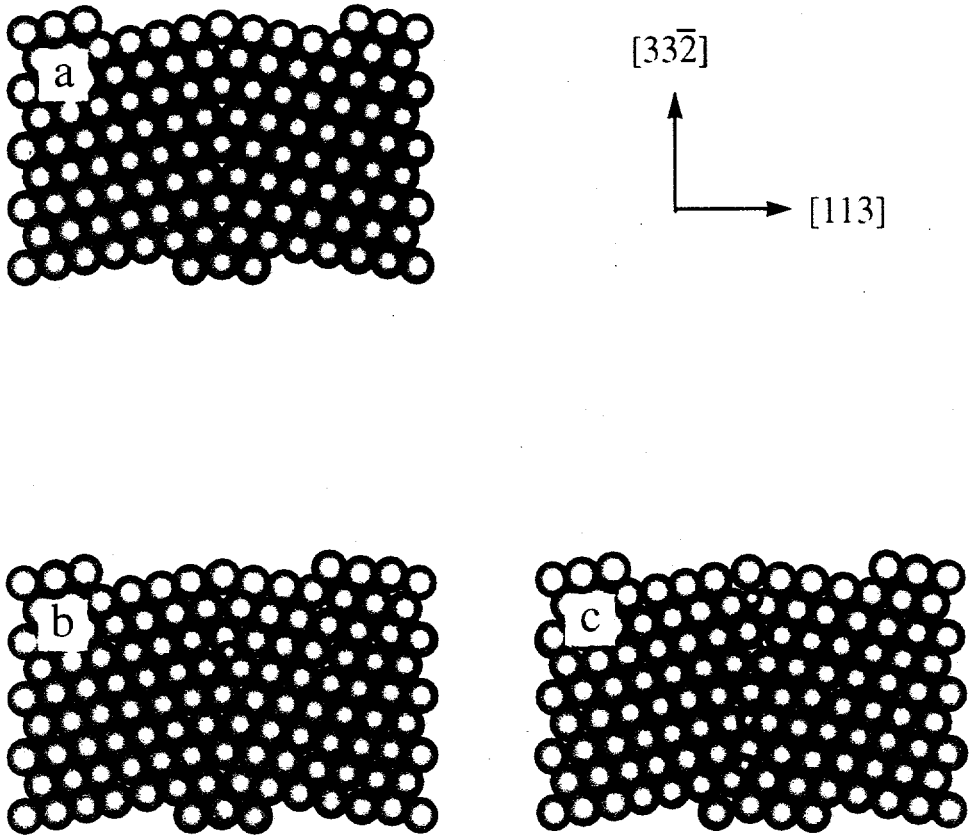

Figure 5: The minimum energy boundary structure for the $\Sigma 11(113)$ tilt boundary is symmetric as indicated in (a). Segregation behavior of hydrogen to this boundary is indicated in (b) and (c) for far-field hydrogen concentration of 23 appm and 446 appm, respectively. The high energy trap sites at the boundary are saturated at the low far-field hydrogen concentrations. In (b) and (c) hydrogen is indicated by the small balls.

minimum energy structure, but rather to the local minimum. In order to determine the true minimum energy structure the crystals were displaced past each other by varying amounts prior to relaxation, and the energy of each relaxed configuration compared. This procedure produced the relaxed $\Sigma 3$ boundary shown in figure 4(a) showing that the boundary has become asymmetric upon relaxation. The lattices have sheared by 0.05 nm

parallel to the boundary and by 0.125 (a/4[110]) nm along the tilt axis. This shearing produced a relaxed boundary structure which had an energy that was 320 ergs/cm^2 lower than the relaxed symmetric boundary structure. The relaxed boundary structure for the $\Sigma 11$ tilt boundary is shown in figure 5(a). For this boundary, the minimum energy structure was symmetric and not very different from the ideal boundary structure. The differing relaxation behavior is most likely associated with the observation that the atomic density in the {113} planes is higher than that in the {112} planes. This behavior is consistent with experimental observations in gold [28] as well as theoretical predictions for fcc metals [29,30].

Exposing the grain boundary structures to a hydrogen environment showed a similar effect for both the $\Sigma 3$ and $\Sigma 11$ tilt boundaries. In both cases, the high energy trap sites at the boundary were nearly saturated with hydrogen at a far-field hydrogen concentration of 23 appm. This trapping is shown in figure 4(b) for the $\Sigma 3$ boundary. Similar results for the $\Sigma 11$ tilt boundary are shown in figure 5(b). Exposure of the boundary structures to a higher far-field hydrogen concentration (446 appm) caused near boundary trap sites to fill with hydrogen with little increase in the hydrogen trapped immediately at the boundary plane. The boundary structures showed a slightly different segregation behavior at this far-field concentration. Typical examples, at a far-field concentration of 446 appm, for both the $\Sigma 3$ and $\Sigma 11$ boundaries are shown in figures 4(c) and 5(c), respectively. The $\Sigma 3$ boundary showed a slightly asymmetric segregation behavior owing to the fact that the minimum energy boundary structure was asymmetric. In contrast, the segregation of hydrogen to the $\Sigma 11$ tilt boundary was more symmetric reflecting the boundary structure (hence trap site distribution) for this boundary. For both boundaries there was significant solubility enhancement, even for the far-field hydrogen concentration of 23 appm. Here the solubility enhancement was determined by averaging the amount of hydrogen in a volume extending to 2.0 nm on either side of the boundary. For the $\Sigma 3$ boundary, the solubility enhancement at the boundary was 1000 and 122 for the far-field hydrogen concentrations of 23 and 446 appm, respectively. Meanwhile solubility enhancements of 473 and 78.8 were observed at the $\Sigma 11$ boundary for the same far-field hydrogen concentrations. The slightly larger solubility at the $\Sigma 3$ boundary is associated with a larger excess volume at this boundary.

III. Discussion and Conclusions

The controlling mechanism of hydrogen embrittlement in the fcc metals is an elusive phenomena with the divergent HEDE and HELP models both having support from the experimental literature. This study was initiated in an effort to better understand the energies which characterize the trapping of hydrogen to lattice defects in nickel. The trapping of hydrogen to the edge and screw dislocations is associated with a binding energy of 0.09-0.12 eV in excellent agreement with the observed trap binding energy measured in nickel [25]. This is significantly less than the experimentally observed activation energy of 0.3-0.4 eV for trap site induced hydrogen embrittlement as measured using fracture toughness data obtained by Moody et al. [31] for IN903. This energy is similar to that found for the trapping of hydrogen to the Lomer-Cottrell Lock and to all of the tilt boundaries modeled in this study. Here, it has been found using Monte-Carlo simulations that hydrogen does indeed segregate strongly to both the LCL and tilt boundaries in nickel, and to a much lesser extent to edge and screw dislocations. In previous works [12-14], it was also shown that the segregation of hydrogen to grain boundaries severely decreased the brittle work of fracture for these grain boundaries in nickel. This effect was caused by saturation of the high energy trap sites along the grain boundary. An increase in the far-field hydrogen content caused an increase in the near boundary hydrogen concentration, but had little effect on the fracture behavior. This

suggests that when the high energy trap sites at the grain boundary are occupied, the effect of hydrogen on the fracture properties has been determined. In this study the high energy trap sites at both boundaries saturate at 23 appm far-field hydrogen so that the observed embrittlement with high hydrogen concentrations would not be caused by simple grain boundary failure. It thus appears that the trapping of hydrogen to the LCL's might play a significant role in the embrittlement process. Since the LCL's would exist in slip band intersections, and be immobile due to their dissociated state, significant segregation of hydrogen is expected to these dislocations. The segregated hydrogen decreases the strain energy associated with the LCL thus stabilizing it against dislocation pile-up. The increase in stress due to dislocation pile-up against the LCL would cause an increase in the stress concentration nucleating cracks at the slip band intersections. This appears consistent with experimental observations showing that high hydrogen fugacities cause an increase in the propensity for slip band fracture as well as observations of void formation at slip band intersections.

Acknowledgments:

The authors thank Stephen Foiles of Sandia National Laboratories for his many helpful discussions during the course of this study. Critical reviews of this manuscript by Doug Medlin and Daryl Chrzan are also greatly appreciated. This work was supported by the US Department of Energy under contract DE-AC04-94AL85000.

References:

[1] N.R. Moody, S.L. Robinson, and M.W. Perra, in Hydrogen Effects on Material Behavior, edited by N.R. Moody and A.W. Thompson (TMS, Warrendale, PA, 1990) p.625.

[2] W.W. Gerberich and A.G. Wright, in Environmental Degradation of Engineering Materials in Hydrogen, edited by M.R. Louthan, R.P. McNitt, and R.D. Sisson (NASA-NACE, Blacksburg, VA, 1981) p.183.

[3] N.R. Moody, S.L. Robinson, and W.M. Garrison, Res Mechanica, 30, 143 (1990).

[4] N.R. Moody, M.W. Perra, and S.L. Robinson, Scripta Metall. 22, 1261 (1988).

[5] W.W. Gerberich, P. Marsh, J. Hoehn, S. Venkateraman, and H. Huang, Corrosion-Deformation Interactions, edited by T. Magnin and J.M. Gras (les éditions de physique, France 1993) p.325, and references therein.

[6] H.K. Brinbaum, in Hydrogen Effects on Material Behavior, edited by N.R. Moody and A.W. Thompson (TMS, Warrendale, PA, 1990) p.639, and references therein.

[7] W.W. Gerberich and T.J. Foecke, in Hydrogen Effects on Material Behavior, edited by N.R. Moody and A.W. Thompson (TMS, Warrendale, PA, 1990) p.687.

[8] N.R. Moody and S.L. Robinson, Corrosion-Deformation Interactions, edited by T. Magnin and J.M. Gras (les éditions de physique, France 1993) p.389.

[9] S.P. Lynch, Acta Metall., 36, 2639 (1988).

[10] G.M. Bond, I.M. Robertson, and H.K. Birnbaum, Acta Metall., 36, 2193 (1988).

[11] G.M. Bond, I.M. Robertson, and H.K. Birnbaum, Acta Metall., 37, 1407 (1987).

[12] N.R. Moody and S.M. Foiles, in Structure/Property Relationships for Metal/Metal Interfaces, edited by A.D. Roming, D.E. Fowler, and P.D. Bristowe, (Mater. Res. Symp. Proc. 229, Pittsburgh, PA 1991) pp.179-185.

[13] N.R. Moody and S.M. Foiles, in Structure and Properties of Interfaces, edited by W.A.T. Clark, C.L. Briant, and U. Dahmen, (Mater. Res. Symp. Proc. 238, Pittsburgh, PA 1992) p.381.
[14] J.E. Angelo, N.R. Moody, M.I. Baskes, and W.W. Gerberich, 1993 TMS Annual Meeting, Denver, CO (1993).
[15] C.L. Fu and G.S. Painter, J. Mater. Res., 6, 719 (1991).
[16] R.G. Hoagland and H.L. Heinisch, J. Mater. Res., 7, 2080 (1992).
[17] M.S. Daw, M.I. Baskes, C.L. Bisson, and W.G. Wolfer, in Modeling Environmental Effects on Crack Growth Processes, edited by R.H. Jones and W.W. Gerberich, (TMS-AIME, Warrendale, PA 1986) p.99.
[18] P. Sofronis and H.K. Birnbaum, submitted JMPS (1994).
[19] M.S. Daw and M.I. Baskes, Phys. Rev. Lett., 50, 1285 (1983).
[20] M.S. Daw and M.I. Baskes, Phys. Rev. B, 29, 6443 (1984).
[21] M.S. Daw, S.M. Foiles, and M.I. Baskes, Mat. Sci. Reports, 9, 251 (1993).
[22] J.E. Angelo, N.R. Moody, and M.I. Baskes, to be submitted, Modelling Simul. Mater. Sci. Eng. (1994).
[23] S.M. Foiles, in Surface Segregation and Related Phenomena, edited by P.A. Dowben and A. Miller, (CRC Press, Boca Raton, FL 1990) p. 79, and references therein.
[24] A.N. Stroh, Phil. Mag., 3, 625 (1958).
[25] G.J. Thomas, in Hydrogen Effects in Metals, edited by I.M. Bernstein and A.W. Thompson, (Metallurgical Society of AIME, New York, NY 1980) p.77.
[26] D. Hull and D.J. Bacon, in Introduction to Dislocations, 3rd Ed., (Pergamon, Oxford 1989).
[27] J.W. Christian, in The Theory of Transformations in Metals and Alloys, Part I, (Pergamon, Oxford 1981).
[28] K.L. Merkle and D. Wolf, Phil. Mag. A, 65, 513 (1992).
[29] D. Wolf, Acta Metall., 37, 1983 (1989).
[30] D. Wolf, Acta Metall., 37, 2823 (1989).
[31] N.R. Moody, et al., in preparation (1994).

DISCLAIMER